Journal of Energy Chemistry 108 (2025) 165–172

Contents lists available at ScienceDirect

Journal of Energy Chemistry

journal homepage: www.elsevier.com/locate/jechem

http://www.journals.elsevier.com/journal-of-energy-chemistry/

Electron-deficient intermolecular adhesives: a new class of multifunctional interlayers for efficient and stable perovskite solar cells ☆

Gyeong-Ho Jeong [a,1], Gyeong Seok Lee [b,1], Ramesh Kumar Chitumalla [a], Jungkwon OH [c], Jong-Min Kim [a], Dong-Geon Kwun [a], Dong-Hwan Hwang [a], In Hwa Cho [d], Da In Kim [b], Wolfgang Tress [e], Joonkyung Jang [a], O-Pil Kwon [c,*], Yun-Hi Kim [b,*], Ji-Youn Seo [a,*]

[a] Department of Nano Fusion Technology, Pusan National University, Busan 46241, Republic of Korea
[b] Department of Chemistry and RIMA, Gyeongsang National University, Jinju 52828, Republic of Korea
[c] Department of Molecular Science and Technology, Ajou University, Suwon 16499, Republic of Korea
[d] Department of Nano-semiconductor Process & Equipments, Pusan National University, Busan 46241, Republic of Korea
[e] Institute of Computational Physics, Zurich University of Applied Sciences, Wildbachstr. 21, 8401 Winterthur, Switzerland

ARTICLE INFO

Article history:
Received 30 January 2025
Revised 21 March 2025
Accepted 1 April 2025
Available online 18 April 2025

Keywords:
C_{60} interface adhesion
Perovskite Solar Cells
Electron-deficient intermolecular adhesives
Interfacial engineering

ABSTRACT

Since 2009, perovskite solar cells (PSCs) have advanced significantly, achieving over 26% efficiency for single-junction devices and exceeding 34% for silicon-perovskite tandem cells. Despite these successes, the weak adhesion of C_{60} to perovskite layers, due to van der Waals interactions, hinders long-term stability. In this study, we introduce electron-deficient intermolecular adhesives (EDIAs) as a novel interlayer material to enhance adhesion between perovskite and C_{60} layers. Comprehensive analyses, including density functional theory calculations, microscopy, and spectroscopy, demonstrate that EDIAs, particularly NDI-C9-Ace comprising of three key functionalities: a π-electron-deficient arene core, a hydrophobic passivation core, and a secondary-bond anchoring core, significantly improve bonding strength and recombination passivation. This leads to enhanced efficiency as well as enhanced mechanical and photochemical stability in PSCs. Long-term stability tests further confirm the superior durability of EDIA-enhanced devices. This study highlights EDIA as a promising strategy for enhancing the robustness and efficiency of PSCs.

1. Introduction

Since 2009, thanks to the efforts of many researchers, perovskite solar cells (PSCs) have matured into a highly advanced technology, achieving efficiencies of over 26% for single-junction devices and over 34% for silicon tandem solar cells [1,2]. Due to these excellent performance metrics and economic viability, many solar cell companies around the world are preparing for commercialization. In particular, existing silicon solar cell companies are investing heavily in the commercialization of silicon-perovskite tandem solar cells. Among the various structures being researched for the development of tandem cells with silicon solar cells, the p-i-n (inverted) structure is the most widely studied [3–5]. The most commonly used electron transport material (ETM) in p-i-n PSCs is C_{60}, due to its superior electrical properties and ideal band alignment [6,7]. Additionally, when applied via vacuum deposition, C_{60} offers the advantage of uniform coating over large areas, making it suitable for use in silicon-PSCs [7–9].

However, a notable drawback of C_{60} is its weak adhesion when deposited on the perovskite layer due to van der Waals interactions, which can lead to delamination under external stress conditions such as impact, bending, and/or thermal expansion, ultimately reducing long-term stability [7,10,11]. Although various

☆ This article is part of a special issue entitled: 'Celebrate the 80th birthday of Prof. M. Graetzel' published in Journal of Energy Chemistry.

* Corresponding authors.
E-mail addresses: opilkwon@ajou.ac.kr (O-Pil Kwon), ykim@gnu.ac.kr (Y.-H. Kim), j-y.seo@pusan.ac.kr (J.-Y. Seo).

[1] These authors contributed equally to this work.

https://doi.org/10.1016/j.jechem.2025.04.012

electron transport layer (ETL) materials have been developed to overcome this issue, none have yet proven to surpass C_{60} in terms of both performance and cost-effectiveness. To overcome this limitation, this study introduces a novel class of interlayer materials, termed electron-deficient intermolecular adhesives (EDIAs). EDIAs are specifically designed to concurrently enhance electronic and mechanical adhesion between the perovskite layer and C_{60} while maintaining the latter's excellent and advantageous properties. To elucidate the electrical properties of the newly designed EDIAs, we performed density functional theory (DFT) calculations and applied the material to perovskite, followed by characterization using atomic force microscopy (AFM), electrostatic force microscopy (EFM), Kelvin probe force microscopy (KPFM), X-ray photoelectron spectroscopy (XPS), and ultraviolet photoelectron spectroscopy (UPS). Additionally, Fourier transform infrared (FTIR) spectroscopy, bending tests, scanning electron microscopy (SEM) observations, photoluminescence (PL), and impedance spectroscopy analyses, confirmed that EDIA materials significantly improve the bonding strength with both C_{60} and perovskite, as well as provide effective recombination passivation. Furthermore, through the fabrication of EDIA-incorporated solar cell devices, we achieved enhanced efficiency and long-term stability.

2. Experimental

2.1. Materials

[4-(3,6-dimethoxy-9H-carbazol-9-yl)butyl]phosphonic acid (MeO-4PACz) was supplied from TCI, Japan. Cesium Iodide (CsI) was prepared from Sigma-Aldrich, USA. Formamidinium Iodide (FAI) and Formamidinium bromide (FABr) were purchased from GreatCell Solar, Australia. Lead Iodide (PbI_2) and Lead bromide ($PbBr_2$) were supplied from TCI, Japan. Fullerene (C_{60}) was prepared from nanoC, USA, and Bathocuproine (BCP) was purchased from TCI, Japan. Silver (Ag) pellets were supplied by iTASCO, Korea. All reagents and solvents were purchased from commercial suppliers, including Aldrich Inc., Tokyo Chemical Industry Co., Ltd. (TCI), and Alfa Aesar. 9-amino-1-nonanol and 11-Amino-1-undecanol were synthesized using previously reported synthetic methods [12,13].

2.2. Sample preparation

For films analyses, each film was fabricated as follows. $Cs_{0.17}FA_{0.83}Pb(I_{0.88}Br_{0.12})_3$ was prepared first. CsI, FAI, FABr, PbI_2, and $PbBr_2$ powders were dissolved in DD solution (DMF (Sigma-Aldrich, USA):DMSO = 9:1) 1.47 M concentration following composition mentioned at first. All solutions were stirred for 2 h. Glass substrates were prepared by ultrasonic cleaning in Hellmanex Ⅲ (Sigma-Aldrich, USA), followed by sequential cleaning with deionized water (DI water), isopropyl alcohol (IPA) (Daejung Chem, Korea), and ethanol (EtOH) (Daejung Chem, Korea). The cleaned glass substrates were then dried at 120 ℃ on a hotplate. After drying, the glass substrates were treated with oxygen plasma (100 W, 80 sccm, and 60 s; COVANCE, Femto Science, Hwaseong-si, 18469, Korea) for 15 min before use. All the solutions and films were fabricated in a nitrogen-filled glovebox. The perovskite precursor solution was spread and spin-coated onto the glass substrates with 7 s acceleration until 2000 rpm and kept for 3 s. After spin coating, the substrates were immediately transferred to a vacuum chamber and exposed to a vacuum for 20 s. After vacuum flushing, the substrates were transferred to a hotplate and annealed at 100 ℃ for 20 min. NDI-C11 or NDI-C9-Ace was dissolved in chlorobenzene (Sigma-Aldrich, USA) at a concentration of 0.7 mg/mL and dropped onto the perovskite film. After 10 s of wetting, spin-coating was performed at 2000 rpm for 20 s. After spin-coating, the film was annealed at 100 ℃ for 10 min on a hotplate. To prepare the ETL, C_{60} was deposited using a thermal evaporator under a high vacuum (10^{-6} Torr (1 Torr = 133.322 Pa)) to a thickness of approximately 25 nm.

For device fabrication, Indium-doped tin oxide (ITO, AMG, Korea) glass was cleaned using ultrasonic cleaning in Hellmanex Ⅲ, DI water, IPA, and EtOH, sequentially, and then dried at 120 ℃ on a hotplate. The cleaned ITO glass was subsequently treated with oxygen plasma for 15 min before use. The hole transporting layer (HTL) was prepared on ITO glass by spin-coating the MeO-4PACz solution at 2000 r/min for 30 s, followed by annealing at 100 ℃ for 10 min on a hotplate. The perovskite precursor solution was prepared and fabricated following the same procedure as for film fabrication. NDI-C9-Ace or NDI-C11, and the ETL were also deposited using the same method as in film fabrication. The BCP buffer layer was deposited onto the C_{60} film by a thermal evaporator under a high vacuum (10^{-6} Torr) to a thickness of approximately 3 nm. Finally, Ag as a top electrode was deposited using a thermal evaporator under a high vacuum (10^{-6} Torr) to a thickness of approximately 100 nm, to complete the device with an Ag pellet. For long-term stability characterization, a maximum power point tracking (MPPT) system was utilized. To fabricate MPPT samples of PSCs, an aluminum oxide (Al_2O_3) passivation layer was deposited using atomic layer deposition (ALD). Trimethylaluminum (TMA, iChems Co., Korea) and H_2O were used as the aluminum and oxygen precursors, respectively. The ALD process was performed at a substrate temperature of 60 °C and a chamber pressure of 1 Torr. Each ALD cycle consisted of a 1-second TMA exposure, followed by a 10-second Ar purge, a 1-second H_2O exposure, and a 15-second Ar purge. This sequence was repeated for 250 cycles to achieve a uniform and conformal Al_2O_3 thin film.

3. Results and discussion

3.1. π-electron deficient intermolecular adhesives

Fig. 1(a) illustrates three different functionalities in EDIA materials, acting as electronic and mechanical adhesives for both the ETL and perovskite layers. EDIA molecules consist of a π-electron deficient arene core and a secondary-bond anchoring core that are linked with a hydrophobic passivation core. The π-electron deficient arene cores exhibit intermolecular (and interionic) multiple-interaction capabilities. The electron-withdrawing groups (EWGs) on arene cores result in the formation of π-electron deficient parts possessing partially positive charge (δ^+). The partially positive charge (δ^+) groups can form intermolecular interaction with electron-rich (δ^-) groups (e.g., anion and π-rich group). In addition to partially positive charge (δ^+) groups, partially negative charge (δ^-) of π-electron rich parts coexist and can interact with electron-deficient (δ^+) groups (e.g., cation and π-hole group).

In this work, the naphthalene diimide (NDI) group is chosen for π-electron deficient arene cores [15–21]. The four imide EWGs create π-electron deficient (δ^+) characteristics of two diimide rings on NDI (Fig. 1b) [18–21]. The details of the computational study in Fig. 1 are described in Supporting Information (SI). The π-electron deficient (δ^+) characteristics on NDI strongly interact with several (partially) negative charge (δ^-) groups in electron transport C_{60} and perovskite materials. Fig. 1(c) shows the electrostatic potential of ETM C_{60} that exhibits two opposite partial charges: (δ^+) δ-hole [5.6] bonds and (δ^-) δ-rich [6.6] bonds [22–25]. In the perovskite layer (FAPbI3 in Fig. 1d), iodide anions and lead (and FA) cations co-exist. Consequently, π-electron deficient (δ^+) groups on NDI may form intermolecular interactions with π-rich bonds

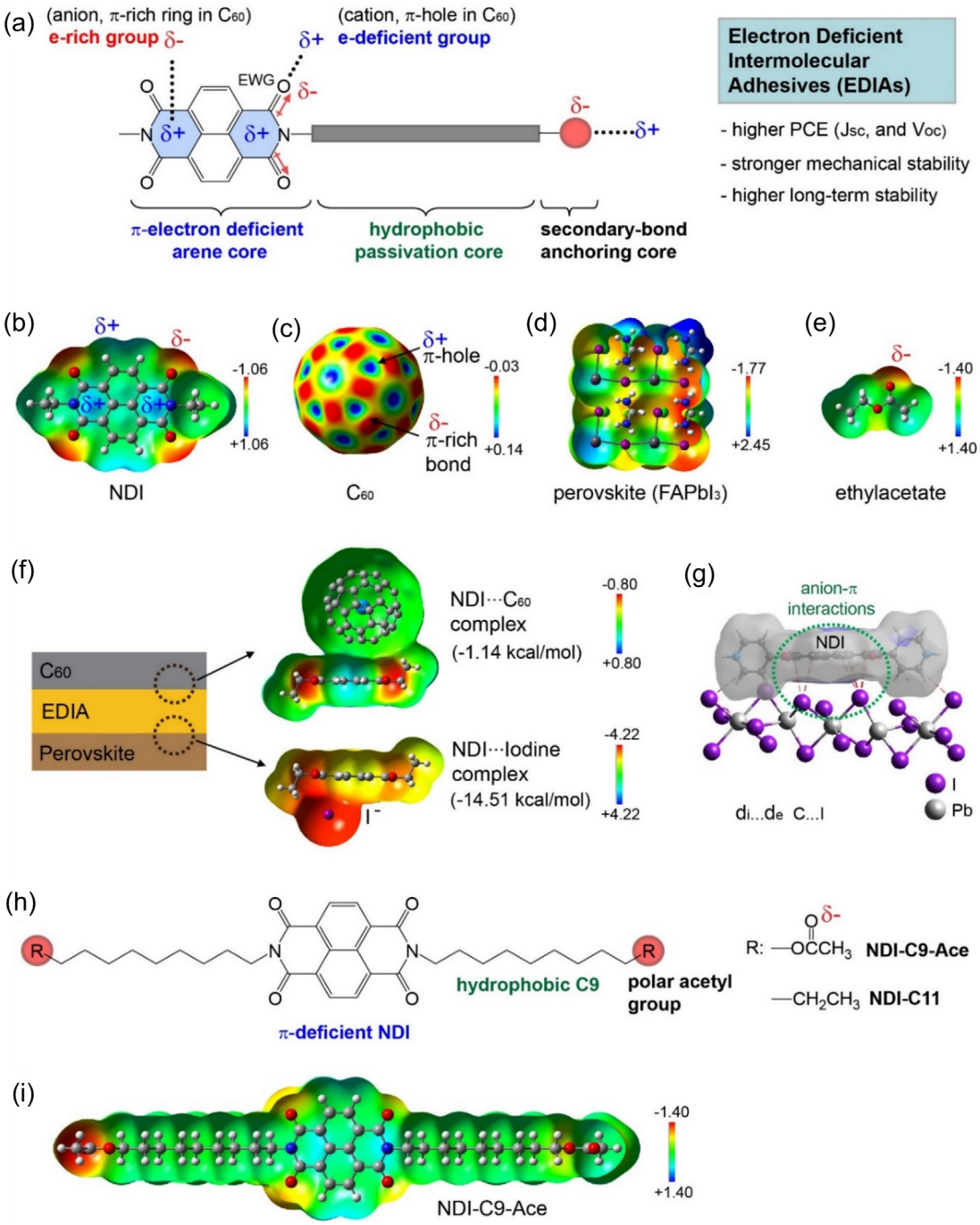

Fig. 1. (a) Schematic of π-electron deficient intermolecular adhesives (EDIAs). Electrostatic potentials of (b) N-ethyl NDI, (c) C_{60}, (d) perovskite (top view of PbI-terminated surface of $FAPbI_3$ here), (e) ethyl acetate, and (f) NDI···C_{60} and NDI···I^- complexes (scale bar unit: eV). (g) Example of NDI···iodine complex, presenting with Hirshfeld surface of with atom contact C···I [14]. The red dotted lines present C···I with a distance of <4.0 Å [14]. (h) Chemical structure and (i) electrostatic potential (scale bar unit: eV) of EDIAs in this work.

(δ^-) on C_{60} (Fig. 1c) and then lead to the formation of NDI···C_{60} complex with stabilization energy of −1.14 kcal/mol (Fig. 1f) [26,27]. In addition, π-electron deficient (δ^+) groups on NDI may form the NDI···I- complex with a high stabilization energy of −14.51 kcal/mol (Fig. 1h) which is an analogue of strong π···anion interactions [16,28–30]. Note that strong interactions between NDI derivatives and halide (including iodine) ions in many crystalline solids have previously been observed [14,31–34]. One example of NDI···iodine complex in a solid, with a Hirshfeld surface, is presented in Fig. 1(f) [35]. The crystal structure is obtained from Ref. [14]. In addition to π-electron deficient (δ^+) groups on NDI, hydrogen substituents on the aromatic ring (Ar-H) exhibit additional (δ^+) characteristics (Fig. 1b). This additionally interacts with (δ^-) δ-rich [6.6] bonds on C_{60} and anions on perovskite.

In the EDIA molecule, a secondary-bond anchoring core is introduced (Fig. 1a). In this study, a polar acetyl group is chosen as the secondary-bond anchoring core (Fig. 1h). Fig. 1(e) shows the electrostatic potential of the acetyl group (ethyl acetate). The electronegativity χ^G of the acetate group is very high, (χ^G = 3.04), while χ^G = 2.52 for the alkyl (ethyl) group [36]. The partially

negative charge (δ^-) ester group on the acetyl group within the acetyl moiety can interact with (δ^+) δ-hole [5.6] bonds in C_{60} and Pb^{2+} (and FA) cations in perovskite layers. In addition, the methyl group on the acetyl moiety that possesses a partially positive charge (δ^+) (Fig. 1e), can interact with several partially negative charge (δ^-) groups, as discussed above. Moreover, the C=O groups on 4 imide EWGs in NDI cores exhibit additional (δ^-) characteristics (Fig. 1b) similar to the secondary-bond anchoring core and therefore can interact with (δ^+) δ-hole [5.6] bonds in C_{60} and Pb^{2+} (and FA) cations in perovskite layers.

Fig. 1(h) shows the chemical structure of two EDIA molecules used in this work and experimental details on molecular synthesis and analysis are in SI (Figs. S1–S11). While NDI-C9-Ace consists of a π-electron deficient NDIs, hydrophobic passivation $-(CH_2)_9-$ groups, and secondary-bond anchoring acetyl (Ace) groups, NDI-C11 lacks the polar acetyl groups. In this study, two distinct EDIA molecules were used as interlayers between the perovskite and ETL. As discussed above, the NDI-C9-Ace (and NDI-C11) molecule possesses intermolecular (and interionic) multiple-interaction capabilities (Fig. 1i) and forms complexes of NDI···C_{60} and NDI···I^- (Fig. 1f). Therefore, in terms of electronic properties, these complexes may result in better electron injection and transport properties, leading to increased current density (J_{sc}), open-circuit voltage (V_{oc}), and power conversion efficiency (PCE). In addition, these strong interactions may also result in increased mechanical (and photochemical) stability. On the other hand, the alkyl groups with weak interaction ability on EDIA molecules may act as hydrophobic passivation groups against humidity. Therefore, EDIA materials in this study might act as electronic and mechanical adhesives for both C_{60} ETL and perovskite layers.

3.2. Modification of electrical and adhesive properties

We analyzed the changes in the electrical and mechanical properties of perovskite films after coating their surfaces with EDIAs, utilizing AFM and SEM techniques. As depicted in Fig. 2(a–c), the application of EDIAs significantly reduced the surface roughness compared to the pristine perovskite surface. As expected, the EDIAs formed a uniform layer on the perovskite surface, resulting in a reduction in surface roughness. Notably, NDI-C9-Ace exhibited greater improvement in surface flatness compared to NDI-C11, likely due to its stronger binding affinity to the perovskite layer and more stable adhesion facilitated by anchoring acetyl (Ace) groups.

In addition to the enhancement of surface morphology, we also observed changes in electrical properties through EFM measurements (Fig. 2g–j). Electrostatic force (EF) is generally originated by accumulated surface charge. Moreover, this kind of EF decreases the electric device's conductivity. As is well known, conductivity in pristine perovskite films tends to decrease at grain boundaries and similar regions [37,38]. However, surfaces coated with EDIAs exhibited remarkably uniform and low EF signal, with NDI-C9-Ace showing particularly pronounced uniformity. This improved surface condition is expected to facilitate stable charge transport with the ETL C_{60}. To further investigate whether the changes in surface electrical properties influence the work function, we performed KPFM (Fig. S12) and UPS (Fig. S13) analyses on the same samples. To investigate how the surface modification effect of EDIAs influences the performance of solar cell devices, we fabricated full PSCs as shown in Fig. 3(a). Since device performance is significantly affected by both the bandgap alignment and charge recombination at interfaces, we conducted analyses prior to device performance testing to examine the impact of surface modification on these factors. Using UPS and optical spectroscopy techniques (including ultraviolet–visible (UV–vis) absorption and photoluminescence) (see details in Figs. S13 and S14, Table S1), we observed changes in band alignment and electron recombination, as illustrated in Fig. 3(b) and (c). The results revealed that in the samples with EDIAs applied, both the highest occupied molecular orbital (HOMO) and the lowest unoccupied molecular orbital (LUMO) levels shifted to deeper positions, leading to a change in the work function. This confirmed that the work function was indeed modified, thereby enhancing the n-type properties of the ETL in the EDIA-treated samples. The NDI-C9-Ace film, with a thickness of less than 10 nm, allows electron tunneling due to its deep HOMO level, effectively preventing recombination. In Fig. 3(c), steady-state PL measurements were performed to compare charge transport characteristics in samples with and without EDIAs. When EDIAs were coated on the perovskite, a blue shift accompanied by a quenching effect was observed. However, the most notable effect occurred when EDIAs were inserted between the perovskite and C_{60} layers. In this configuration, EDIAs mitigated the quenching effect more effectively than when only C_{60} was deposited on the perovskite. To further examine this behavior, the average radiative recombination lifetime (τ_{avg}) was determined through TRPL fitting, as shown in Fig. S15. The results indicate that NDI-C9-Ace extended the exciton lifetime in PSCs, suggesting reduced interfacial recombination when NDI-C9-Ace was applied. To verify the passivation effect of EDIAs, recombination resistance was analyzed using impedance spectroscopy (IS), with data fitted to an equivalent circuit model (Fig. S16). Across the entire voltage range, NDI-C9-Ace exhibited the highest recombination resistance, reaffirming its effectiveness in suppressing recombination. Non-radiative recombination, where energy is dissipated as heat, contrasts with radiative recombination, which can be re-utilized through interactions such as refraction, reflection, or scattering within thin films [39]. As the number of interfaces increases, non-radiative recombination naturally becomes more prevalent. However, minimizing this quenching effect is crucial for achieving high-efficiency solar cells. In this regard, incorporating EDIAs between the perovskite and C_{60} layers further reduces quenching, enhancing the potential for improved device performance [39–41]. To investigate the charge extraction properties of NDI-C9-Ace in PSC devices, external quantum efficiency (EQE) was measured (Fig. S17). The EQE data reveal that NDI-C9-Ace demonstrated superior photon-to-electron conversion efficiency in the 350–450 nm range compared to both the pristine sample and NDI-C11. This improvement is likely attributed to the absorption and emission characteristics of NDI-C9-Ace in this specific spectral region (Fig. S10), allowing for more effective utilization of these wavelengths. To further examine molecular-level binding interactions, an XPS analysis was performed, focusing on surface chemical interactions. To get depth atomic information, XPS depth profiling was utilized with an Ar^+ ion etching process at 100 s intervals. The interface was defined as the region where C, I, and Pb have inclinations as the etching progresses. The bulk was defined as the region where I and Pb keep the prior ratio although the etching progresses. The surface data were measured before etching. Interface data were measured near the cross point of C and Pb. Bulk data were measured near the cross point of Pb and Br (Fig. S18). The presence of C_{60} resulted in clearly detected C 1*s* peaks (Fig. S19a), while weak Pb 4*f* and I 3*d* signals were observed from the underlying perovskite film (Fig. 3d, g). After calibrating the spectra within a 0.1 eV error margin based on the C 1*s* peak, no significant changes were noted in the I 3*d* and Pb 4*f* peaks at the surface. However, when EDIAs were applied at the perovskite/C_{60} interface, strong intermolecular binding was detected. This was evidenced by a 0.4 eV shift in the I 3d peaks (Fig. 3e) and a 0.3–0.4 eV shift of the Pb 4*f* peaks to higher binding energy (Fig. 3h). In the perovskite bulk region, there were no significant changes in the I 3*d* and Pb 4*f* peaks (Fig. 3f, i). It is clear to distinguish each depth region because a metallic Pb 4*f* peak is observed

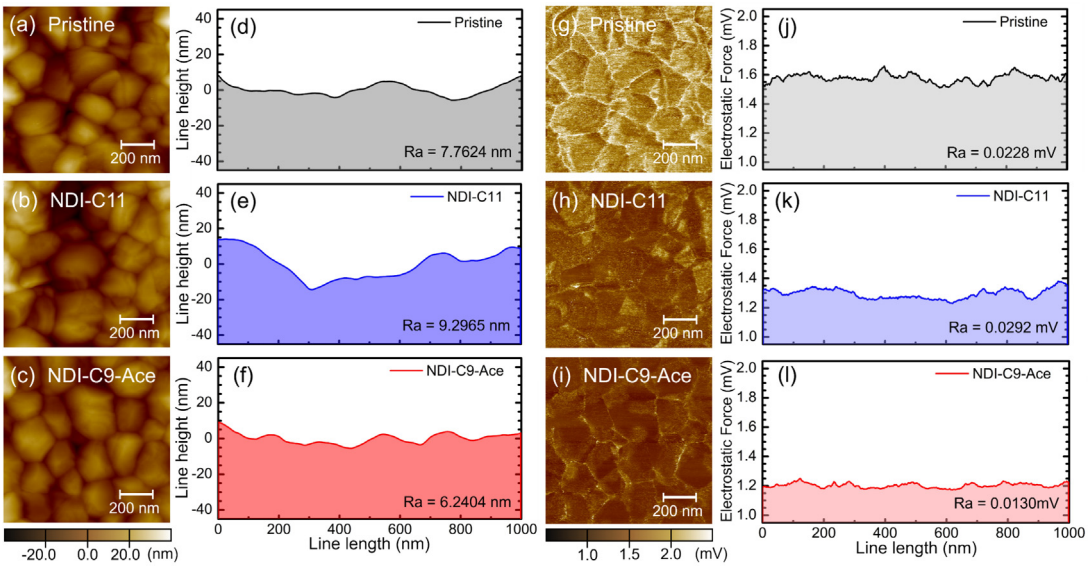

Fig. 2. (a–c) Surface morphology of bare perovskite, perovskite coated with NDI-C11, and perovskite coated with NDI-C9-Ace. (d–f) Cross-sectional profiles of each film condition corresponding to images (a–c). (g–i) EFM images, and (j–l) electrostatic force profiles of each film condition.

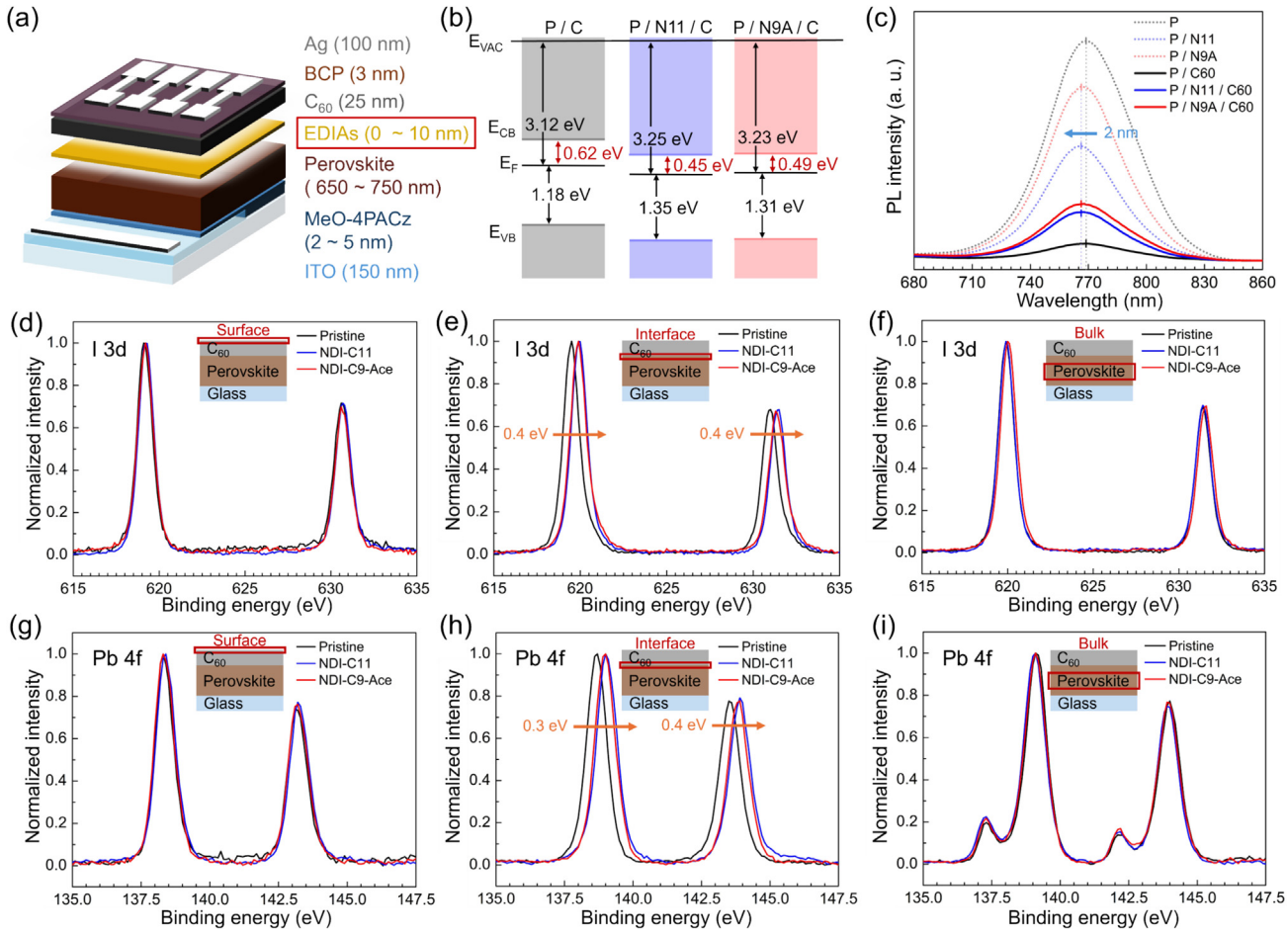

Fig. 3. (a) Device structure of perovskite solar cells device. (b) Schematic band diagram of three conditions. Perovskite film (P) and C_{60} film (C) were deposited on the Si wafer in order. NDI-11 (N11) or NDI-C9-Ace (N9A) film was coated between the two films. (c) PL spectrum of each condition. XPS spectra of the I 3*d* orbital at the (d) surface, (e) interface, and (f) bulk region, and the Pb 4*f* orbital at the (g) surface, (h) interface, and (i) bulk region, obtained from the perovskite and C60 films through depth profiling.

in perovskite bulk. Furthermore, weak Br 3*d* peaks were shown at the surface (Fig. S19b) and relatively clear Br 3*d* peaks were detected at the bulk (Fig. S19j). Consequently, Br 3*d* peaks were rarely detected at the interface (Fig. S19f), as they do not significantly interact between the perovskite and C_{60} layers. Additionally, N 1*s* and O 1 *s* peaks were observed also under all conditions. As a

result, weak signals were detected at the surface likely due to surface oxidation in ambient air, as shown in Fig. S19(c, d). FTIR analysis was also performed for each condition (Fig. S20). Although no prominent differences were observed in Fig. S20(b, c), the N–H stretching (3,200–3,500 cm^{-1}), C–N stretching (800–1,000 cm^{-1}), and C–H bending (700–800 cm^{-1}) peaks were weakened when NDI-C11 was applied between the perovskite and C_{60} layers (Fig. S20d). In contrast, these signals were offset and reinforced when NDI-C9-Ace was applied at the same interface. This suggests that long carbon chains in NDI-C11 can hinder chemical bonding when C_{60} is deposited, particularly in the absence of secondary anchoring groups.

To prove this effect, additional DFT calculations were performed. Considering the aggregation effect, we calculated the dimerization energy (ΔE_d) of each EDIA. Since the π-π interaction is expected to be the strongest, most EDIAs would stack in the same direction and other conformations of EDIAs would not interact significantly. As a result, NDI-C11 (ΔE_d = −20.84 kcal/mol) prefers a dimer state over NDI-C9-Ace (ΔE_d = −20.11 kcal/mol) and this energy difference could affect formation energy (−1.14 kcal/mol) of NDI···C_{60} complex, as shown in Fig. S21(a, b) and Fig. 1f. Furthermore, the alkyl chain in NDI-C11 can freely rotate because it is formed by carbon–carbon single bonds (Fig. S21c). In contrast, the free rotation of the alkyl chain in NDI-C9-Ace would be restricted, as acetyl groups could form four hydrogen bonds (Fig. S21d). AFM study was also conducted for each condition. C_{60} was effectively deposited on the perovskite film but spotty at pristine conditions (Fig. S22a). NDI-C11 could disturb C_{60} deposition on perovskite film, as shown in Fig. S22(b), even though it can still attract C_{60} due to the π-π interaction. NDI-C9-Ace, on the other hand, attracts C_{60} via the π-π interaction and forms a dense, smooth surface, even though C_{60} was not deposited locally (Fig. S22c). According to EFM measurement, even though stable EF of C_{60} film was measured at pristine and NDI-C9-Ace conditions (Fig. S22d, f), unstable EF of C_{60} film was measured at NDI-C11 condition (Fig. S22e) without sample bias. In addition, when a 1 V sample bias was applied, the NDI-C9-Ace condition showed the highest activated EF property, which could affect the higher voltage property (Fig. S22g–i). These results show the important role of the secondary anchoring group in EDIAs.

To further assess the impact of molecular-level adhesion on mechanical stability, we conducted a bending test on flexible devices with C_{60} deposited on perovskite films containing EDIAs and analyzed the surface using SEM, as shown in Fig. 4. For comparison, the surfaces were also examined before the bending test (Fig. 4a–c). As the number of bending cycles increased, cracks became increasingly pronounced (Fig. 4d-i). Under pristine conditions, both the perovskite and C_{60} layers exhibited significant cracking, as shown in Fig. 4(d, g) [42,43]. Similarly, samples with NDI-C11 displayed extensive cracking, similar to the pristine samples (Fig. 4e, h). In contrast, samples treated with NDI-C9-Ace, which exhibits strong intermolecular binding, showed significantly fewer and narrower cracks (Fig. 4f, i). Additional SEM images from different regions and magnifications (Figs. S23 and S24) confirmed this trend. Notably, in the NDI-C9-Ace-treated samples, cracks were discontinuous and localized, suggesting that the NDI backbone and secondary anchoring groups effectively shield the perovskite layer. Moreover, the NDI's arene core enhances adhesion to C_{60}, further stabilizing the interface. These results demonstrate that strong molecular interactions significantly enhance bulk film bonding properties, contributing to improved mechanical stability under stress.

3.3. Perovskite solar cell performance

To assess the effect of NDI-C9-Ace on PSC performance, we fabricated devices with and without EDIAs. The PCEs of PSC devices, measured under standard AM 1.5G 1-sun conditions, showed an enhancement when EDIAs were employed, as depicted in the statistical photovoltaic (PV) box chart in Fig. 5(a–d) (summarized in Table 1). The champion device with NDI-C9-Ace achieved an improved efficiency of 21.96%, compared to 21.10% for the pristine sample. This improvement was primarily attributed to increases in V_{oc} and FF, with a more pronounced improvement in V_{oc}, due to the

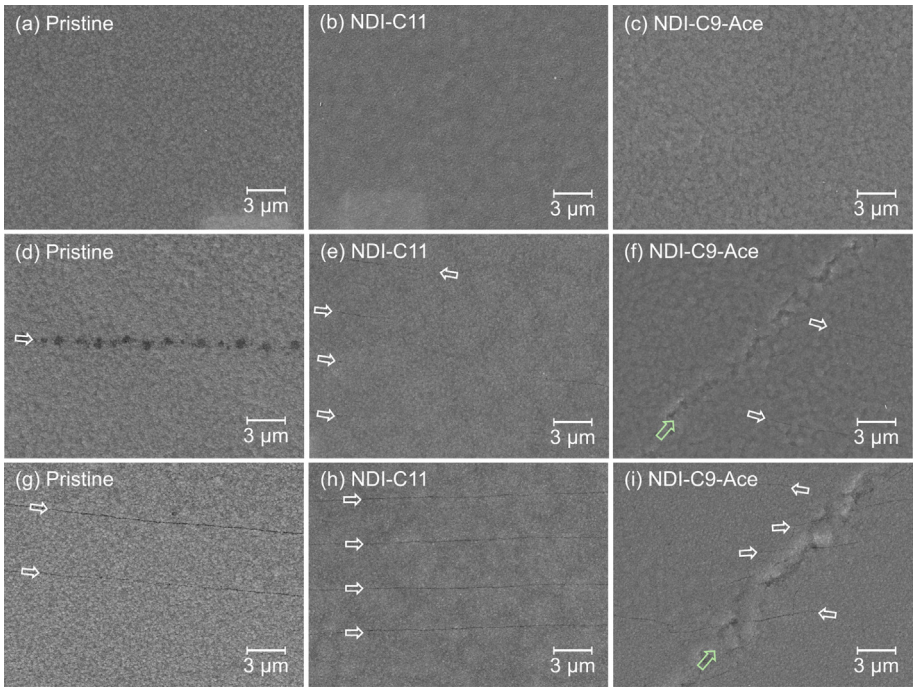

Fig. 4. Surface morphology of each condition (a) C_{60} deposited on perovskite (b) NDI-C11 coated between perovskite and C_{60} (c) NDI-C9-Ace coated between perovskite and C_{60}. (d–f) Surface morphology of each film condition after 15,000 times of bending test. (g–i) Surface morphology of each film condition after 20,000 times of bending test.

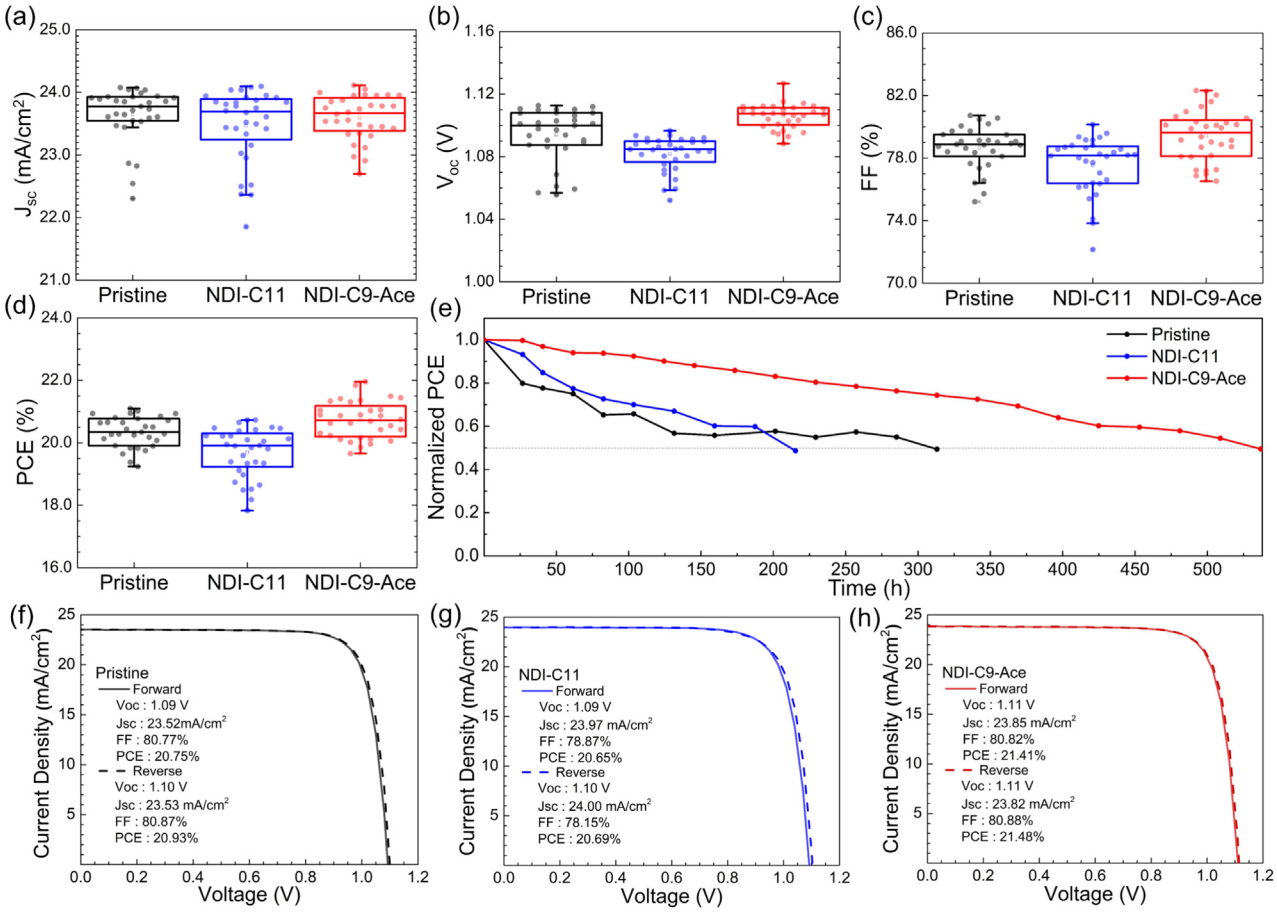

Fig. 5. (a–d) Statistical data of PV parameter under AM 1.5 illumination. 32 data were extracted from each device condition. (e) Normalized maximum power point tracking measurement results after fitting. Encapsulated devices were exposed under AM 1.5 illumination at 25 °C, RH 40%. Hysteresis *J-V* curve of champion PSCs: (f) pristine, (g) NDI-C11, and (h) NDI-C9-Ace.

Table 1
Photovoltaic parameters of PSC devices derived from *J-V* curves measured under AM 1.5 1 sun illumination.

	J_{sc} (mA/cm^2)	V_{oc} (V)	FF (%)	PCE (%)
Pristine	23.94 (23.64)	1.10 (1.09)	80.05 (78.66)	21.10 (20.35)
NDI-C11	23.92 (23.47)	1.09 (1.08)	79.59 (77.55)	20.73 (19.69)
NDI-C9-Ace	23.68 (23.60)	1.13 (1.11)	82.28 (79.43)	21.96 (20.73)

passivation effect confirmed by PL and IS analyses. In addition, DFT calculations and EFM analysis also support these results. Even though the NDI backbone could work as a multi-functional molecule, a long alkyl chain can disturb the interaction between each molecule without a secondary anchoring group (Figs. S21 and S22). Because it would induce decreased electrical performance, EDIAs must be formed with 3 functional components as shown in Fig. 1(a). For the evaluation of long-term operational stability, encapsulated devices were subjected to measurements under continuous 1-sun illumination using an LED light soaking chamber. The device incorporating NDI-C9-Ace exhibited significantly enhanced stability, maintaining higher performance metrics compared to the control device without EDIAs, as shown in Fig. 5e. This improvement is attributed to the presence of the acetyl group in NDI-C9-Ace, which facilitates stable anchoring interactions with the perovskite surface. In contrast, NDI-C11, which lacks an anchoring functional group, exhibited a less uniform morphology on the perovskite surface, as observed in the AFM images in Fig. 2. This weaker interfacial interaction likely contributed to its inferior stability under continuous illumination and bias stress conditions. Hysteresis behavior was also evaluated (Fig. 5f–h), revealing that NDI-C9-Ace provided slightly more stable characteristics in both the flat and slope regions of the *J-V* curve. Hysteresis can typically result from factors such as ion migration, poor charge carrier mobility, or inefficient charge injection. Ion vacancies caused by ion migration can also lead to charge traps, promoting recombination. As discussed in Fig. 1(f, g), EDIA materials help suppress ion migration by forming complexes with iodine and C_{60}, thereby reducing recombination. These effects further explain the improved performance and recombination suppression observed in the PSCs, as shown in Fig. 3(b, c) and Figs. S15 and S16 [44,45].

4. Conclusions

In conclusion, this study introduces a novel class of multifunctional interlayer materials, EDIAs, designed to enhance both electronic and mechanical adhesion at the perovskite/C_{60} interface in PSCs. Through an extensive suite of characterizations, including

DFT simulations, advanced microscopy, spectroscopy, and mechanical stability assessments, we demonstrated that EDIA materials, particularly NDI-C9-Ace, significantly reinforce interfacial bonding while providing effective passivation. These enhancements result in improved device performance, including higher PCE and prolonged operational stability. Long-term stability tests under continuous illumination further confirmed that devices with NDI-C9-Ace exhibit superior durability compared to those without EDIAs, validating its potential for real-world application. This work establishes a foundation for the development of more stable and efficient PSCs, advancing the commercialization prospects of this next-generation photovoltaic technology.

CRediT authorship contribution statement

Gyeong-Ho Jeong: Writing – review & editing, Writing – original draft, Methodology, Investigation, Formal analysis, Data curation. **Gyeong Seok Lee:** Writing – original draft, Visualization, Formal analysis, Data curation. **Ramesh Kumar Chitumalla:** Writing – original draft, Validation, Formal analysis. **Jungkwon OH:** Writing – original draft, Formal analysis, Data curation. **Jong-Min Kim:** Validation, Investigation, Formal analysis. **Dong-Geon Kwun:** Investigation, Formal analysis. **Dong-Hwan Hwang:** Formal analysis. **In Hwa Cho:** Validation, Supervision, Investigation, Formal analysis. **Da In Kim:** Investigation, Formal analysis, Data curation. **Wolfgang Tress:** Writing – original draft, Validation, Supervision, Formal analysis. **Joonkyung Jang:** Supervision. **O-Pil Kwon:** Writing – review & editing, Writing – original draft, Validation, Supervision, Conceptualization. **Yun-Hi Kim:** Writing – review & editing, Writing – original draft, Supervision, Investigation, Conceptualization. **Ji-Youn Seo:** Writing – review & editing, Writing – original draft, Supervision, Project administration, Methodology, Investigation, Funding acquisition, Formal analysis, Conceptualization.

Declaration of competing interest

The authors declare that they have no known competing financial interests or personal relationships that could have appeared to influence the work reported in this paper.

Acknowledgments

J.-Y. Seo and O-P. Kwon are grateful to the Ministry of Trade, Industry and Energy (MOTIE) and Korea Institute for Advancement of Technology (KIAT) through the International Cooperative R&D program (P0026100). This study was supported by National Research Foundation of Korea (NRF) (RS-2024-00336766 and RS-2023-00301974). J. Jang acknowledges the support of the National Research Foundation of Korea (NRF) grant funded by the Korea government (MSIT) (RS-2023-00220748).

Appendix A. Supplementary material

Supplementary data to this article can be found online at https://doi.org/10.1016/j.jechem.2025.04.012.

References

[1] Z. Liang, Y. Zhang, H. Xu, W. Chen, B. Liu, J. Zhang, H. Zhang, Z. Wang, D.H. Kang, J. Zeng, X. Gao, Q. Wang, H. Hu, H. Zhou, X. Cai, X. Tian, P. Reiss, B. Xu, T. Kirchartz, Z. Xiao, S. Dai, N.G. Park, J. Ye, X. Pan, Nature 624 (2023) 557–563.
[2] E. Ugur, A.A. Said, P. Dally, S. Zhang, C.E. Petoukhoff, D. Rosas-Villalva, S. Zhumagali, B.K. Yildirim, A. Razzaq, S. Sarwade, A. Yazmaciyan, D. Baran, F. Laquai, C. Deger, I. Yavuz, T.G. Allen, E. Aydin, S. De Wolf, Science 385 (2024) 533–538.
[3] Y.H. Lin, N. Sakai, P. Da, J. Wu, H.C. Sansom, A.J. Ramadan, S. MA, J. Liu, R.D.J. Oliver, J. Lim, L. Aspitarte, K. Sharma, P.K. Madhu, A.B. Morales-Vilches, P.K. Nayak, S. Bai, F. Gao, C.R.M. Grovenor, M.B. Johnston, J.G. Labram, J.R. Durrant, J.M. Ball, B. Wenger, B. Stannowski, Science 369 (2020) 96–102.
[4] X. Li, W. Zhang, X. Guo, C. Lu, J. Wei, J. Fang, Science 375 (2022) 434–437.
[5] Q. Jiang, J. Tong, Y. Xian, R.A. Kerner, S.P. Dunfield, C. Xiao, R.A. Scheidt, D. Kuciauskas, X. Wang, M.P. Hautzinger, R. Tirawat, M.C. Beard, D.P. Fenning, J.J. Berry, B.W. Larson, Y. Yan, K. Zhu, Nature 611 (2022) 278–283.
[6] C. Chen, P. Zhu, X. Dong, Y. Dou, Y. Zhang, J. Liang, R. Mao, Y. Jiang, J. Wang, M. Wang, S. Chen, J. Zhu, Chem. Eng. J. 489 (2024) 151403.
[7] A.A. Said, E. Aydin, E. Ugur, Z. Xu, C. Deger, B. Vishal, A. Vlk, P. Dally, B.K. Yildirim, R. Azmi, J. Liu, E.A. Jackson, H.M. Johnson, M. Gui, H. Richter, A.R. Pininti, H. Bristow, M. Babics, A. Razzaq, T.G. Allen, M. Ledinsky, I. Yavuz, B.P. Rand, S. De Wolf, Nat. Commun. 15 (2024) 708.
[8] R. Lin, J. Xu, M. Wei, Y. Wang, Z. Qin, Z. Liu, J. Wu, K. Xiao, B. Chen, S.M. Park, G. Chen, H.R. Atapattu, K.R. Graham, J. Xu, J. Zhu, L. Li, C. Zhang, E.H. Sargent, H. Tan, Nature 603 (2022) 73–78.
[9] A. Al-Ashouri, E. Kohnen, B. Li, A. Magomedov, H. Hempel, P. Caprioglio, J.A. Marquez, A.B. Morales Vilches, E. Kasparavicius, J.A. Smith, N. Phung, D. Menzel, M. Grischek, L. Kegelmann, D. Skroblin, C. Gollwitzer, T. Malinauskas, M. Jost, G. Matic, B. Rech, R. Schlatmann, M. Topic, L. Korte, A. Abate, B. Stannowski, D. Neher, M. Stolterfoht, T. Unold, V. Getautis, S. Albrecht, Science 370 (2020) 1300–1309.
[10] C.C. Boyd, R. Cheacharoen, T. Leijtens, M.D. McGehee, Chem. Rev. 119 (2019) 3418–3451.
[11] F. Ye, S. Zhang, J. Warby, J. Wu, E. Gutierrez-Partida, F. Lang, S. Shah, E. Saglamkaya, B. Sun, F. Zu, S. Shoaee, H. Wang, B. Stiller, D. Neher, W.H. Zhu, M. Stolterfoht, Y. Wu, Nat. Commun. 13 (2022) 7454.
[12] D.J. Yoo, K.-S. Lee, A.R. Kim, K.S. Nahm, Korean. Chem. Eng. Res. 49 (2011) 330–337.
[13] C. Chen, P. Yang, S. Wang, S. Tung, W. Su, Macromolecules 19 (2018) 51.
[14] J.J. Liu, Y.F. Guan, C. Jiao, M.J. Lin, C.C. Huang, W.X. Dai, Dalton Trans. 44 (2015) 5957–5960.
[15] S.V. Bhosale, C.H. Jani, S.J. Langford, Chem. Soc. Rev. 37 (2008) 331–342.
[16] S. Guha, F.S. Goodson, L.J. Corson, S. Saha, J. Am. Chem. Soc. 134 (2012) 13679–13691.
[17] B.M. Oh, S.H. Park, J.H. Lee, J.C. Kim, J.B. Lee, H.J. Eun, Y.S. Lee, B.E. Seo, W. Yoon, J.E. Kwon, H. Yun, S.K. Kwak, O.P. Kwon, J.H. Kim, Adv. Funct. Mater. 31 (2021) 2308036.
[18] M.S. Cubberley, B.L. Iverson, J. Am. Chem. Soc. 123 (2001) 7560–7563.
[19] C.R. Martinez, B.L. Iverson, Chem. Sci. 3 (2012) 2191–2201.
[20] M.L.N. Pina, M.S. Gutierrez, M. Panagos, P. Duel, A. Leon, J. Morey, D. Quinonero, A. Frontera, RSC Adv. 9 (2019) 24184–24191.
[21] H.C. Henriksen, A.J. Sowers, C.R. Travis, T.D. Vulpis, T.A. Cope, S.K. Ouslander, A. F. Russell, M.R. Gagne, V. Pophristic, Z. Liu, M.L. Waters, J. Am. Chem. Soc. 145 (2023) 27672–27679.
[22] P.L. Rodriguez-Kessler, N.D. Charistos, R.B. King, A. Munoz-Castro, Phys. Chem. Chem. Phys. 22 (2020) 14268–14275.
[23] A. Miralrio, L.E. Sansores, B. King, A. Munoz-Castro, Phys. Chem. Chem. Phys. 20 (2018) 26325–26332.
[24] Y.B. Wang, Z. Lin, J. Am. Chem. Soc. 125 (2003) 6072–6073.
[25] C. Pesado-Gómez, J.S. Serrano-García, A. Amaya-Flórez, G. Pesado-Gómez, A. Soto-Contreras, D. Morales-Morales, R. Colorado-Peralta, Coord. Chem. Rev. 501 (2024) 215550.
[26] K.M. Bak, I. Marques, H. Kuhn, K.E. Christensen, V. Felix, P.D. Beer, J. Am. Chem. Soc. 145 (2023) 27367–27379.
[27] Y. Zhao, Y. Cotelle, L. Liu, J. Lopez-Andarias, A.B. Bornhof, M. Akamatsu, N. Sakai, S. Matile, Acc. Chem. Res. 51 (2018) 2255–2263.
[28] I.A. Rather, S.A. Wagay, R. Ali, Coord. Chem. Rev. 415 (2020) 213327.
[29] B.L. Schottel, H.T. Chifotides, K.R. Dunbar, Chem. Soc. Rev. 37 (2008) 68–83.
[30] M. Giese, M. Albrecht, K. Rissanen, Chem. Rev. 115 (2015) 8867–8895.
[31] J.-J. Liu, S.-B. Xia, T. Liu, C.-X. He, H. Suo, J. Liu, J. Solid State Chem. 295 (2021) 121900.
[32] S.Q. Zhang, H. Fang, F.H. Chen, M.J. Lin, Inorg. Chem. 62 (2023) 19706–19719.
[33] J.J. Liu, Y.F. Guan, Y. Chen, M.J. Lin, C.C. Huang, W.X. Dai, Dalton Trans. 44 (2015) 17312–17317.
[34] J.J. Liu, Y.J. Hong, Y.F. Guan, M.J. Lin, C.C. Huang, W.X. Dai, Dalton Trans. 44 (2015) 653–658.
[35] A.V. Parwani, Yearbook of Pathology and Laboratory Medicine. 2009 (2009) 93–95.
[36] C.H. Suresh, N. Koga, J. Am. Chem. Soc. 124 (2002) 1790–1797.
[37] Z. Chu, M. Yang, P. Schulz, D. Wu, X. Ma, E. Seifert, L. Sun, X. Li, K. Zhu, K. Lai, Nat. Commun. 8 (2017) 2230.
[38] A.F. Castro-Méndez, J. Hidalgo, J.P. Correa-Baena, Adv. Energy Mater. 9 (2019) 1901489.
[39] W. Tress, Adv. Energy Mater. 7 (2017) 1602358.
[40] Y. Tian, A. Merdasa, M. Peter, M. Abdellah, K. Zheng, C.S. Ponseca Jr., T. Pullerits, A. Yartsev, V. Sundstrom, I.G. Scheblykin, Nano Lett. 15 (2015) 1603–1608.
[41] O.D. Miller, E. Yablonovitch, S.R. Kurtz, IEEE J. Photovoltaics. 2 (2012) 303–311.
[42] M. De Bastiani, G. Armaroli, R. Jalmood, L. Ferlauto, X. Li, R. Tao, G.T. Harrison, M.K. Eswaran, R. Azmi, M. Babics, A.S. Subbiah, E. Aydin, T.G. Allen, C. Combe, T. Cramer, D. Baran, U. Schwingenschlögl, G. Lubineau, D. Cavalcoli, S. De Wolf, ACS Energy Lett. 7 (2022) 827–833.
[43] G.A. Olah, I. Bucsi, R. Aniszfeld, G.K.S. Prakash, Carbon 8 (1992) 1203–1211.
[44] W. Tress, J Phys Chem Lett. 8 (2017) 3106–3114.
[45] W. Tress, N. Marinova, T. Moehl, S.M. Zakeeruddin, M.K. Nazeeruddin, M. Grätzel, Energ. Environ. Sci. 8 (2015) 995–1004.